1904 2004

Concrete — A Century of Innovation

ACI Sub-Committee 544-E

Mechanical Properties of FRCs

Agenda

Monday, March 19, 2012

5:00 PM – 6:30 PM

Hyatt Regency Dallas
Dallas, TX
Room: Gaston B

1. Call to Order and Approval of the Agenda

2. Introductions

3. Review of the TAC Review:
   a) Report on the "*Indirect Method for Obtaining a Model Stress-Strain Curve of Strain Softening FRCs*"
   b) Technical Note on FRC Nomenclature and Acronym.

4. Future Topics and Documents
   - Ultra High Performance FRC and new ACI 239 Committee on Ultra High Performance Concrete

5. New Business

6. Adjourn

SECOND ANNOUNCEMENT AND CALL FOR PAPERS

BMC-10

10th International Symposium on

BRITTLE MATRIX COMPOSITES

October 15-17, 2012

Staszic Palace
Warsaw, Poland

Institute of Fundamental Technological Research
Polish Academy of Sciences

RILEM co-sponsorship

General

The BMC is a tri-annual symposium focusing on the research, development and application of different composite materials with matrices behaving as brittle under normal or special conditions. The present Symposium follows the series of highly successful meetings which originated with EUROMECH 204 Colloquium on Brittle Matrix Composites held in Jablonna, Poland, in November 1985. This meeting was later renamed BMC 1. The Second Symposium (BMC 2) was held in Cedzyna, Poland, in September 1988. Starting with the 1991 meeting (BMC 3) all subsequent BMC Symposia were held every three years in Warsaw, Poland.

Warsaw

The City of Warsaw is the cultural, entertainment and financial capital of Poland. Warsaw is a city with the "enchanted soul" and the ambiance produced by attractive combination of modern urban development and historical architecture. Warsaw's mixture of architectural styles reflects the turbulent history of the city and country.

Venue

The Symposium will be held in the Staszic Palace located in the center of Warsaw. The Palace is situated at a walking distance from the several hotels where the participants can seek accommodations. The sessions will take place in the Mirror Hall, located on the 1st floor of the building.

Exhibition

An informal exhibition of books, papers, magazines, etc., relevant to the Symposium theme will be held in the foyer adjacent to the Mirror Hall. Further information are available upon request.

Travel and Accommodation

The Global Wings Travel Agency has been selected by the organizers to assist with special travel packages, accommodations and post-meeting trips. Further information will be posted on the Symposium website **http://bmc.ippt.gov.pl**

BMC-10 *Pre-registration Form*

October 15 – 17, 2012, Warsaw, Poland

Surname: _____

First name: _____

Title (Prof/Dr/Mr/Mrs/Ms):_____ Male: _____Female: _____

Organization: _____

Address: _____

Number Street

_____

City Province State

_____

Postal Code Country

Tel: _____Fax: _____

Email: _____

Please indicate your intention below:

□ I intend to submit an abstract with the following tentative title:

_____

_____

□ I will not submit an abstract but I plan to attend the Symposium.

□ I am not sure about attending, but keep me on the mailing list.

□ I need information on the exhibition program.

Date:_____ Signature:_____

Please complete and return to:

BMC-10 Symposium Secretariat
Dr. Daria Jóźwiak-Niedźwiedzka
IFTR, 5B Pawinskiego Str.,
02-106 Warszawa, Poland

phone: (+48) 22 8263143, 22 8261281 ext. 217, 310
fax: (+48) 22 8269815
e-mail: abrandt@ippt.gov.pl
djozwiak@ippt.gov.pl

SYMPOSIUM CO-CHAIRMEN

Prof. Dr. A. M. Brandt, Warsaw (Poland)
Prof. Dr. C. K. Y. Leung, Hong Kong (China)
Prof. Dr. J. Olek, West Lafayette (USA)
Prof. Dr. M. A. Glinicki, Warsaw (Poland)

INTERNATIONAL ADVISORY PANEL:

R. Al-Mahaidi, Melbourne (Australia)
A. Bentur, Haifa (Israel)
J.J. Biernacki, Cookeville, TN (USA)
N. De Belie, Gent (Belgium)
R. Gettu, Madras, (India)
A. Klemm, Glasgow (UK)
D. A. Lange, Urbana-Champaign, IL (USA)
S. Mindess, Vancouver (Canada)
Z. Mróz, Warsaw (Poland)
Y. Ohama, Yokohama (Japan)
M. Ohtsu, Kumamoto (Japan)
H.W. Reinhardt, Stuttgart (Germany)
F. Sanchez, Nashville, TN (USA)
S.P. Shah, Evanston, IL (USA)
H. Stang, Lyngby (Denmark)
P. Stroeven, Delft (The Netherlands)
R.N. Swamy, Sheffield (UK)
R.D. Toledo Filho, Rio de Janeiro (Brazil)
Shilang Xu, Hangzhou (China)

CORRESPONDENCE AND INQUIRIES

BMC-10 Symposium Secretariat
Dr. Daria Jóźwiak-Niedźwiedzka
Institute of Fundamental Technological Research
Polish Academy of Sciences
5B Pawinskiego Str.,
02-106 Warszawa, Poland

phone: (+48) 22 8263143, 22 8261281 ext. 217, 310
fax: (+48) 22 8269815
e-mail: abrandt@ippt.gov.pl
djozwiak@ippt.gov.pl

Symposium web site:
http://bmc.ippt.gov.pl

Papers are invited in the following broad areas:

- Mineralogy and microstructure
- Hydration
- Durability, sustainability
- Interactions of cement paste with aggregates and reinforcement
- Cement extending and replacement materials
- High strength composites with brittle matrices
- Sintered materials (ceramics)
- Design and optimization of the structure of materials
- Theoretical considerations and computational methods
- Models of materials and prediction of their properties
- Tests methods and new test results
- Manufacturing processes

Types of contributions

Papers are requested on all aspects of brittle matrix composites. Papers submitted in English must be original, previously unpublished and should advance knowledge and/or technology of the subject. Papers will be presented and discussed only in English. Abstracts and final papers will be reviewed by the Symposium Organizing Committee in conjunction with its International Advisory Panel, composed of world known specialists in the concerned fields. Participants without papers are also warmly invited.

Time Table

In order to ensure that the printed copy of the Proceedings is available at the Symposium the authors are must comply with the following timetable. Those interested in submitting the paper should send Dr. D. Jóźwiak-Niedźwiedzka an abstract (max. 500 words) which should outline (in sufficient details) the contents of the proposed paper and clearly indicate the advances made. The Proceedings will be published both in a hardback form and in the electronic form (CD-ROM) and will be available at the Symposium.

Submission of abstracts:	**November 4, 2011**
Notification of abstracts' acceptance:	**December 31, 2011**
Full length papers due:	**May 7, 2012**
Final papers acceptance:	**June 29, 2012**

Registration fee

Registration type	Early bird Before 31/7/12	Standard After 1/8/12
Participant	500 €	600 €
Students	300 €	350 €
Accompanying persons	200 €	250 €

Registration Fee Includes:
Technical sessions
Bound copy of conference proceedings
Morning and afternoon teas
Lunches
Optional half-day tour *Climates of old and modern Warsaw*
Welcoming cocktail, Sunday, October 14, 2012
Formal dinner, Monday, October 15, 2012
Dinner, Tuesday, October 16, 2012
Closing Banquet, Wednesday, October 17, 2012

Information on registration and available accommodations will be posted on the symposium website.

http://bmc.ippt.gov.pl

POST-SYMPOSIUM SEMINAR
is planned to be organized
IN CRACOW, OCTOBER 18-20, 2012

Multiscale Computational Modeling of Cementitious Materials

Topic 1 – Molecular and atomistic methods;
Topic 2 – Chemical kinetics and microstructure prediction methods;
Topic 3 – Multi-component and multi-phase reactive transport modeling;
Topic 4 – Mechanical property prediction methods;
Topic 5 – Thermo-chemo-mechanical coupling methods;
Topic 6 – Multiscale computational principles and scale bridging methods.

Separate registration fee required

Let us know your interest in participation ☺

ACI 544 – Approved Ballot on FRC Nomenclature

Rev. 1

- **SS-FRC composite or SS-FRCC**: Strain softening fiber reinforced cement (or concrete) composite is classified as a composite material with a tensile stress-strain curve satisfying all of the following requirements:
    1. a primarily linear elastic ascending branch up to the first percolation cracking, followed by
    2. immediate softening after the first percolation cracking where all subsequent stresses remain smaller than the first percolation cracking stress.

  For these cementitious composites, measured strains are valid only up to the first percolation cracking.

- **SH-FRC composite or SH-FRCC**: Strain hardening fiber reinforced cement (or concrete) composite is classified as a composite material with a tensile stress-strain curve satisfying all of the following requirements:
    1. an ascending branch comprised of an initial elastic portion, followed by
    2. a post-elastic portion that is either horizontal or ascending,
    3. the end of the initial ascending portion of the curve exhibits a significant decrease in stiffness, which is indicative of the first percolation cracking,
    4. the peak stress and its corresponding strain are significantly larger than the stress and strain at the first percolation cracking.

  These cementitious composites are likely to generate multiple cracking under tension.

- **DS-FRC composite or DS-FRCC**: Deflection softening fiber reinforced cement (or concrete) composite is classified as a composite material with a load-deflection curve in bending satisfying all of the following requirements:
    1. a primarily linear elastic ascending branch up to the first flexural cracking, followed by
    2. immediate deflection softening after the first flexural cracking where all subsequent loads remain smaller than the first cracking load.

- **DH-FRC composite or DH-FRCC**: Deflection hardening fiber reinforced cement (or concrete) composite is classified as a composite material with a load-deflection curve in bending satisfying all of the following requirements:

    1. an initial elastic portion followed by a post-elastic portion that is either horizontal or ascending,
    2. the end of the initial ascending portion of the curve often exhibits a significant decrease in stiffness, which is indicative of the first flexural cracking,

3. the maximum load or peak load and corresponding deflection are significantly larger than the load and deflection at the first flexural cracking.

These cementitious composites are likely to generate multiple flexural cracks under bending.

Commentary:

a. It should be noted that scale effects are important in the behavior of materials and that in order for a fiber reinforced cement or concrete composite to qualify for a particular classification it should be tested according to acceptable standards such as described by ASTM, Rilem, EN or other recognized international consensus seeking technical organizations.

b. In a slender tensile member subjected to direct tensile loading along its long axis, a percolation crack is a crack that either extends over the entire cross section of the member or whose projection along a plane normal to the loading axis is equal to the cross section of the member, and with a crack boundary that is continuous around the perimeter of the member and such that any point on the crack surface can be reached from any other point using a continuous path.

c. In fiber reinforced concrete test beams that are described in testing standards by ASTM C 1609, Rilem TC 162, EN 14651, or other recognized international consensus seeking technical organization, a flexural crack is one that crosses the entire tensile zone below the neutral axis of bending and extends up to or below the neutral axis of bending.

ACI 544.3R – XXE

Indirect Method for Obtaining a Model Stress-Strain Curve of Strain Softening FRCs

Reported by ACI Committee 544

Nemkumar Banthia
Chair

Neven Krstulovic-Opara*†
Secretary

Melvyn A. Galinat
Membership Secretary

Ashraf Ahmed
Joaquim Oliveira Barros*
Marvin E. Criswell
Ashish Dubey
Sidney Freedman
Antonio J. Guerra
Allen J. Hulshizer
Katherine G. Kuder
Maria Lopez de Murphy
Bruno Massicotte
Barzin Mobasher*
Antonio Nanni
Max L. Porter
Klaus Alexander Rieder
Jim D. Speakman
Jean-François Trottier
Robert C. Zellers

Corina Maria Aldea
Gordon B. Batson
James I. Daniel
Philip J. Dyer
Richard J. Frost
Rishi Gupta
Akm Anwarul Islam
David A. Lange
Clifford N. MacDonald
James R. McConaghy
Henry J. Molloy
Nandakumar Natarajan
John H. Pye
Pierre Rossi
Chris D. Szychowski
George J. Venta
Ronald F. Zollo

Madasamy Arockiasamy
Vivek S. Bindiganavile
Xavier Destree
Gregor Fischer
Graham T. Gilbert
Carol D. Hays
John Jones
John S. Lawler
Pritpal Mangat
Christian Meyer
Dudley R. Morgan
Jeffery Novak
Venkataswamy Ramakrishnan
Surendra P. Shah
Peter C. Tatnall
Gary L. Vondran

P.N. Balaguru
Peter H. Bischoff
Daniel P. Dorfmueller
Dean P. Forgeron
Vellore S. Gopalaratnam
George C. Hoff
Jubum Kim
Mark A. Leppert
Peter Martinez
Nicholas Mitchell
Antoine E. Naaman*
Mark E. Patton
Roy H/ Reiterman
Konstantin Sobolev
Houssam A. Toutanji
Robert Wojtysiak

* Members of the subcommittee who authored this report.
† Chair of the subcommittee who drafted this report.

This document presents existing methods for estimating uniaxial stress-strain response of strain softening FRCs using beam-test data. In this approach uniaxial compressive response is determined directly from standard compression cylinder tests. The uniaxial tensile response is calculated from beam-test data using an approach originally developed by Rilem TC162-TDF committee. The document both (a) provide specific formulas reported in the literature for various beam-test types, (b) and summarizes an inverse-analysis method for obtaining the stress-strain values when test beams differ from those for which the formulas have been develop.

Keywords: beam tests; inverse method; stress-strain relationship; test data analysis; uniaxial tension.

C O N T E N T S

CHAPTER 1 – GENERAL

1.1 – Scope

The document covers existing methods for estimating characteristic tensile stress-strain (or tensile stress crack –width) response of strain softening FRCs using flexural beam-test data. The methods are valid only for strain-softening FRCs, which do not exhibit distributed and parallel microcracking when tested in flexural loading conditions.

1.2 – General

The document presents existing methods for obtaining uniaxial tensile stress-strain curves from beam-test data. In this approach uniaxial compressive response is determined directly from standard compression cylinder tests. The uniaxial tensile response is calculated from flexural load-deflection test-beam data using an approach originally developed by Rilem TC162-TDF committee.

The Rilem TC162-TDF method specifically uses 3-point notched beam tests. The approach outlined herein is presented assuming that any general 3 or 4 point beam-test is used. Values of the necessary coefficients must then be determined from the experimental data using an inverse analysis method. The document both (a) summarizes specific coefficient values reported in the literature for various beam-test types, (b) and provides an inverse-analysis method for obtaining the values when the specific coefficient values are not known.

The document outlines only the calculation method for determining a stress-strain diagram. Statistical aspects of processing actual test data are not addressed here and will be presented elsewhere. It should

also be noted that presented methods have already been validated against experimental data and, therefore, this validation is not presented herein. Additional information on this issue can be obtained from the referenced publications. Finally, this document does not attempt to recommend or favour any of the presented methods. Performance and comparison of the presented methods will be discussed in future publications.

The document first presents (a) a model for equivalent stress strain diagram, (b) calculation procedure for obtaining flexural tensile and residual flexural strengths from beam test data, and (c) a relationship between the parameters that define the stress-strain diagram and the experimentally determined flexural strengths. The relationship is presented in terms of parameterised stress coefficients C_1, C_2, C_3. The coefficients are to be determined using an inverse analysis procedure summarized in chapter 6. Specific coefficient values are provided next for the case of the notched RILEM TC 162-TDF and Belgian NBN B15-238 third-point beams. The coefficient values have not thus far been reported in the literature for other beam types, such as ASTM C1609/C1609M -10, or C1399/C1399M -10 test beams. Therefore, a complete, step-by-step inverse analysis procedure to be used for other beam types is provided in Appendix A.

CHAPTER 2 – NOTATION

b - test beam width (Chapter 3)

C_1, C_2, C_3 - through stress coefficients, calculated from test data using inverse analysis (Chapter 3)

F_L – load level at the limit of proportionality (Chapter 3)

f_r - modulus of rupture (Chapter 3)

$f_{R,1}$ - residual flexural strength at 0.46 mm load-deflection of a RILEM TC 162-TDF test beam (Chapter 3)

$f_{R,4}$ - residual flexural strength at 3.0 mm load-deflection of a RILEM TC 162-TDF test beam (Chapter 3)

$F_{R,1}$ - residual load at 0.46 mm load-deflection of a RILEM TC 162-TDF test beam (Chapter 3)

$F_{R,2}$ - residual load at 3.0 mm load-deflection of a RILEM TC 162-TDF test beam (Chapter 3)

$F_{R\text{-}15}$ - load at 1.5 mm load-deflection of a Belgian Standard NBN B15-238 test beam (Chapter 3)

$F_{R\text{-}30}$ - load at 3 mm load-deflection of a Belgian Standard NBN B15-238 test beam (Chapter 3)

f_t - flexural tensile strength (Chapter 3)

f_{tm} - average value of the flexural tensile strength, i.e., the limit of proportionality of the beam response (Chapter 3)

h_n - net section height of a notched test beam, i.e., distance between the notch tip and the top of the cross-section (Chapter 3)

h_{unc} - uncracked beam height at the limit of proportionality (Chapter 3)

k - neutral axis depth ratio (Chapter 4)

L - test beam span (Chapter 3)

M' - normalized moment obtained by dividing moment M with the cracking moment M_{cr} (Chapter 4)

M'_{bcr} - normalized bilinear cracking moment curvature (see Figure 4 for further definition), (Chapter 4)

M'_{cr} – normalized cracking moment (Chapter 4)

M'_{it} - intersection moment of the linear elastic response and the linear post crack response (see Figure 4 for further definition) (Chapter 4)

M'_u - limit moment that can be used as the ultimate values (see Figure 4 for further definition), (Chapter 4)

S - spacing between the support and the closest loading point (*S=L/2* for three point bending and *S=L/3* for four point bending)

β_{tu} - normalized strain parameters at cracking strain (see Figure 3 for further definition), (Chapter 4)

ε_{cr} - cracking strain (Chapter 4)

ε_{cu} - compressive yield strain defined using scalar parameter λ_{cu} ($\varepsilon_{cu} = \lambda_{cu}\, \varepsilon_{cr}$), (Chapter 4)

ε_{cy} - compressive yield strain defined using scalar parameter ω ($\varepsilon_{cy} = \omega\varepsilon_{cr}$), (Chapter 4)

ε_{tu} - ultimate tensile strain defined using scalar parameter β_{tu}, ($\varepsilon_{tu} = \beta_{tu}\varepsilon_{cr}$), (Chapter 4)

ε_1 – tensile strain at tensile strength (Chapter 3)

ε_2 –strain at the onset of the stable strain softening branch (Chapter 3)

ε_3 –strain at the end of the softening branch (Chapter 3)

ϕ' - normalized curvature obtained by dividing curvature ϕ with the cracking curvature ϕ_{cr} (Chapter 4)

ϕ'_{bcr} - normalized bilinear cracking curvature (see Figure 4 for further definition), (Chapter 4)

ϕ'_{cr} – normalized cracking curvature (Chapter 4)

ϕ'_{it} - intersection curvature of the linear elastic response and the linear post crack response (see Figure 4 for further definition) (Chapter 4)

ϕ'_u - limit curvature that can be used as the ultimate values (see Figure 4 for further definition), (Chapter 4)

λ - normalized strain parameters at cracking strain (see Figure 3 for further definition), (Chapter 4)

λ_{cu} - normalized top compressive strain at compressive failure (Appendix 1)

λ_{tu} - normalized top compressive strain at tensile failure (Appendix 1)

λ_u - ultimate normalized top compressive strain (Appendix 1)

μ - scalar parameter for defining post cracking strength ($\sigma_p = \mu\varepsilon_{cr}E$), (Chapter 4)

μ_{crit} - critical post-crack tensile strength

σ_{cr} – tensile cracking strength (Chapter 4)

σ_{cy} – compressive yield strength defined using scalar parameter ω ($\sigma_{cy} = \omega\varepsilon_{cr}E$), (Chapter 4)

σ_p -post cracking strength in tension defined using scalar parameter μ, ($\sigma_p = \mu\varepsilon_{cr}E$), (Chapter 4)

σ_1 – tensile strength ($\sigma_{cr} = \varepsilon_{cr}E$), (Chapter 3)

σ_2 – stress at the onset of the stable strain softening branch (Chapter 3)

σ_3 – stress at the end of the softening branch (Chapter 3)

ω - normalized strain parameter at cracking strain (see Figure 3 for further definition), (Chapter 4)

5

CHAPTER 3 – METHOD

3.1 – General

Various test methods exist for evaluating directly or indirectly the uniaxial-tensile properties of FRCs. These include uniaxial tensile tests, wedge splitting tests and beam tests. Since beam tests are easier of executing, mainly in conventional field laboratories, the uniaxial-tensile properties of FRCs will be derived from the data of these tests.

Common flexural-beam tests are performed under either (a) 3-point load, such as prescribed by Rilem TC162-TDF and ASTM C293/C293M-10, or (b) 4-point loading conditions, such as prescribed in ASTM C78/C78M-10 (i.e., ASTM C1399/C1399M -10 and C1609 for FRC), DBV 1992, JCI-SF4, NBN B15-238 1992, etc. Beam tests can further be subdivided into notched beams, as is the case with the 3-point load Rilem TC162-TDF test, or un-notched, as is the case with ASTM beams. Use of notched beams decreases significantly data scatter.

Further detailed description of each beam type and test procedure has been presented elsewhere and is, thus, beyond the scope of this document.

3.2 – Stress-Strain Diagram

The stress-strain diagram used in this approach is the same as proposed by RILEM TC 162-TDF [Vandewalle 2003] and shown in Figure 2. The values that define this constitutive model are based on average, or characteristic values which are in turn used in the design purposes.

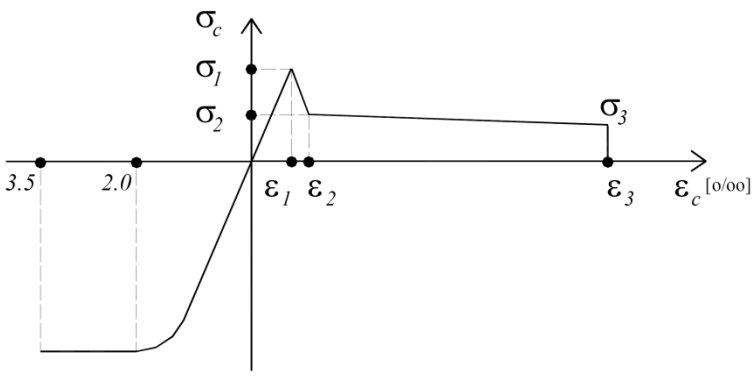

Figure 1: Stress – strain diagram for FRCs in uniaxial tension and compression, according to RILEM TC 162-TDF [Vandewalle 2003].

The key points of the compression side of the diagram are obtained directly from the standard compressive cylinder test. For the tension side of the diagram the key points are (Figure 1):

- σ_1, and ε_1 – tensile strength and corresponding strain
- σ_2, and ε_2 – stress and strain at the onset of the stable strain softening branch
- σ_3, and ε_3 – stress and strain at the end of the softening branch

The values that can be assumed by σ_i (i=1,2,3) can be obtained from the load-displacement response of a test beam [Vandewalle 2000, 2002, Barros 2005]:

- average value of the flexural tensile strength, f_{tm}, i.e., the limit of proportionality of the beam response,
- residual flexural strength at deflection of 0.46 mm, $f_{R,1}$, and
- residual flexural strength at deflection of 3.0 mm, $f_{R,4}$.

Equations to obtain f_{tm}, $f_{R,1}$ and $f_{R,4}$ are indicated in next section, as well as recommendations to estimate ε_i (i=1,2,3) .

3.3 - Calculating Flexural Tensile Strength, f_t, and Residual Flexural Strengths, $f_{R,1}$ and $f_{R,4}$

The flexural tensile strength, f_t, and residual flexural strengths, $f_{R,1}$ and $f_{R,4}$, values are calculated directly from the load displacement response of the test beam, which is schematically represented in Figure 3 ($\delta_{R,1}$=0.46 mm and $\delta_{R,4}$=3.0mm).

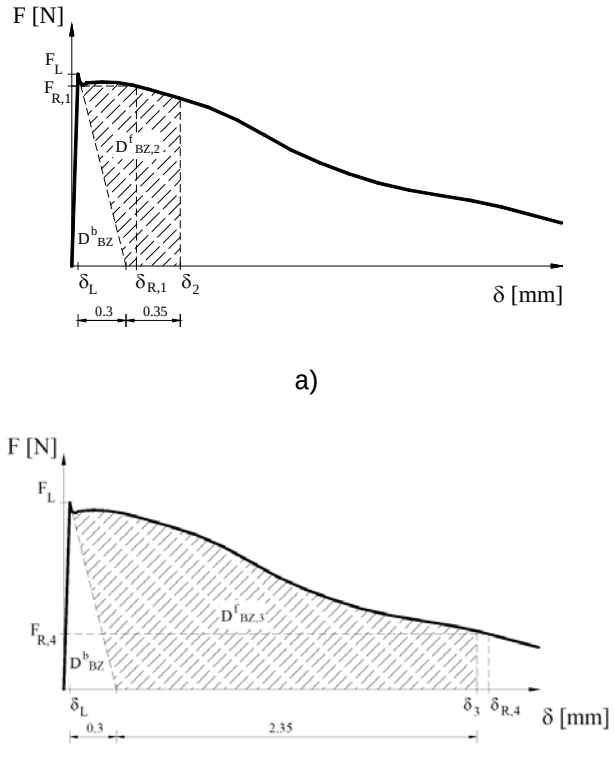

Figure 2: Load – displacement response of a test beam, used in the evaluating of the: a) $f_{R,1}$, b) $f_{R,4}$ [Vandewalle 2000, 2002, Barros 2005].

3.3.1 - Flexural Tensile Strength, f_t

The flexural tensile strength, f_t, is defined as the maximum tensile stress within the critical section at a load level equal to the limit of proportionality, F_L. The limit of proportionality is the load at the end of the linear-elastic response, as shown in Figure 3. However, if there is no clear end point to the linear-elastic portion of the load-displacement curve, the limit of proportionality is then defined as the highest load up to a deflection of 0.05 mm [Vandewalle et al. 2002b].

Similar to the modulus of rupture, f_r, of the conventional concrete materials, the flexural tensile strength, f_t, is calculated assuming linear stress distribution within the critical section. When a three-point beam bending test is used, where variables L, and b define span and width of the test beam, and h_n defines the net section height, the flexural tensile strength, f_t, can be calculated as:

$$f_t = \frac{3F_L L}{2bh_n^2}$$

If a notched test beam is used, the net section height, h_n, equals the distance between the notch tip and the cross-section top.

3.3.2 – Residual Flexural Strengths, f_{r-1} and f_{r-2}

Residual flexural strengths, $f_{R,1}$ and $f_{R,4}$, are obtained from beam loads $F_{R,1}$ and $F_{R,2}$ that correspond to beam deflections of 0.46 and 3.0 mm, respectively [Vandewalle et al. 2002b], as shown in Figure 2. It should be noted that even though at this deflection levels both (a) the stress distribution is no longer linear within the critical section, and (b) the uncracked beam height is smaller than its value at the limit of proportionality, h_{unc}, the same relationship to that used for calculating the flexural tensile strength, f_t, is still used:

$$f_{R,1} = \frac{3F_{R,1} L}{2bh_n^2}$$

$$f_{R,4} = \frac{3F_{R,4} L}{2bh_n^2}$$

3.4 – Relationship Between Uniaxial-Tensile Stresses and Flexural Tensile Strengths

The flexural tensile strength, f_t, and residual flexural strengths, $f_{R,1}$ and $f_{R,4}$, can be directly related to the key tensile stress parameters that define the stress-strain diagram shown in Figure 1. The relationship is

a function of the specimen type and size. The effect of these factors is introduced through stress coefficients C_1, C_2, C_3, calculated from test data using inverse analysis.

3.4.1 – Tensile Stress Values σ_1, σ_2, and σ_3

Tensile stresses values σ_1, σ_2, and σ_3, as defined in Figure 2, can now be calculated as:

$$\sigma_1 = C_1(1.6 - \frac{d}{1.0m}) f_t$$

$$\sigma_2 = C_2 f_{R,1}$$

$$\sigma_2 = C_3 f_{R,4}$$

where all the variables are as defined above.

3.4.2 – Tensile Strain Values ε_1, ε_2, and ε_3

Tensile strain value ε_1, is obtained following the Hook's law and using Young modulus of FRC, E_c, which is assumed to be the same in compression and tension, i.e.:

$$\varepsilon_1 = \frac{\sigma_1}{E_c}$$

All the other strain values, ε_2, and ε_3, must be determined from test data using an inverse analysis procedure.

CHAPTER 4 – EVALUATING STRESS COEFFICIENTS AND STRAIN PARAMETERS

4.1 – Inverse Analysis Procedure for a General Beam Type

The goal of inverse analysis is to determine material properties using experimentally determined moment-deflection response. A spreadsheet based iterative inverse analysis approach presented herein was developed by Soranakom and Mobasher (2006).

Soranakom and Mobasher (2007) used somewhat different nomenclature from that used in Figure 2. The relationship between the two is defined as:

$$\sigma_1 = \sigma_{cr}$$

$$\sigma_2 = \sigma_3 = \sigma_P$$

$$\varepsilon_1 = \varepsilon_2 = \varepsilon_{CR}$$

$$\varepsilon_3 = \varepsilon_{tu}$$

The approach is based on a closed form solution connecting measured flexural response of FRC test beams to assumed material stress-strain response. Tensile stress-strain properties are obtained through an iterative process, as explained next. The procedure has been implemented in an Excel spreadsheet for ease of calculation.

Compressive stress-strain properties are determined from a separate compressive cylinder test. Tensile material parameters are assumed. The moment-curvature diagram is generated next by incrementally increasing the top compressive strain, finding neutral axis and finally calculating moment and curvature. The procedure is repeated until predicted moment-curvature response matches measured values. The readers are advised to consult reference [Soranakom and Mobasher 2006] for in- depth information.

4.1.1 – Material Model

FRC material model used in Soranakom and Mobasher [2007] is shown in Figure 3.

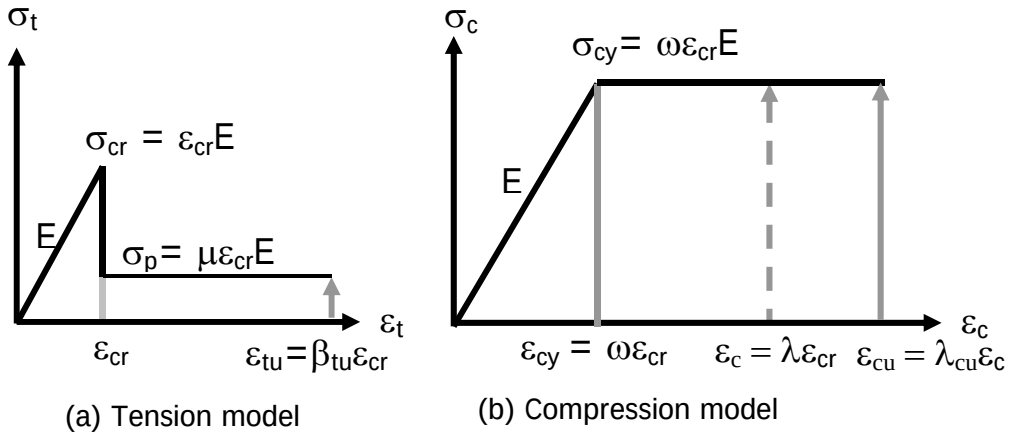

Figure 3: FRC model used by Soranakom and Mobasher [2006].

Following nomenclature is used:

- cracking strength in tension σ_{cr} defined as $\varepsilon_{cr}E$
- post cracking strength in tension, defined using scalar parameter μ, $\sigma_p = \mu\varepsilon_{cr}E$
- ultimate tensile strain ε_{tu} defined using scalar parameter β_{tu}, $\varepsilon_{tu} = \beta_{tu}\varepsilon_{cr}$
- yield strength in compression $\sigma_{cy} = \omega\varepsilon_{cr}E$
- yield strain in compression $\varepsilon_{cy} = \omega\varepsilon_{cr}$
- ultimate compressive strain $\varepsilon_{cu} = \lambda_{cu}\varepsilon_{cr}$

Ultimate tensile and compressive strains are used to limit the flexural strength capacity that the model can potentially provide for FRC members. In this approach all strains and stresses are normalized in terms of the cracking strain ε_{cr}, and cracking strength $\sigma_{cr} = \varepsilon_{cr} E$. Corresponding normalized strain parameters β_{tu}, ω, λ, and λ_{cu}, as well as stress parameters μ and ω, are defined in Figure 3. This strategy has been extended to FRC elements that can also include longitudinally steel and fiber reinforced polymer bars, where ε_2 can be higher than ε_1 and σ_p higher than σ_{cr} in order to simulate strain hardening FRCs (Taheri et al. 2011).

4.1.2 – Moment – Curvature Relationship

Normalized compressive strain at the top fiber λ is selected first. Values are assumed for three different phases: ($0<\lambda\leq 1$), ($1<\lambda\leq\omega$) and ($\omega<\lambda\leq\lambda_{cu}$) representing the three zones of elastic tension-elastic compression, residual strength tension-elastic compression, and residual strength tension-plastic compression phases respectively. The neutral axis depth ratio k is determined next using assumed stress strain diagram and imposing conditions of equilibrium. Corresponding moment of the tension - compression force couple taken around the neutral axis is determined next. Corresponding curvature is determined by dividing the top compressive strain with the neutral axis depth.

Moment M and curvature ϕ are normalized next by dividing them with the cracking moment M_{cr} and cracking curvature ϕ_{cr}, respectively. Obtained values are termed normalized moment M' and curvature ϕ', respectively.

Two simplified moment-curvature diagrams, as shown in Figure 4, are used to optimize the inverse analysis. The intersection points (ϕ'_{it}, M'_{it}) of the linear elastic response and the linear post crack response is determined using the following regression equation:

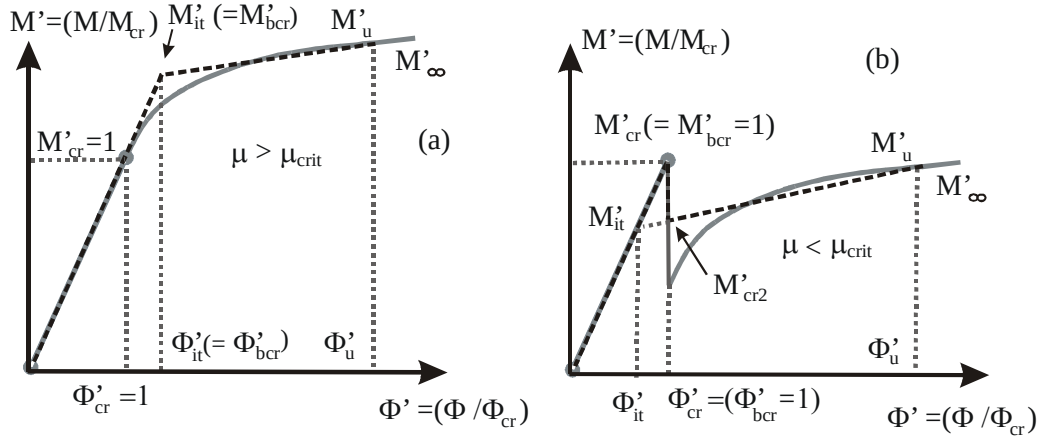

Figure 4: Normalized moment curvature diagrams and their approximate bilinear models: (a) deflection hardening ($\mu > \mu_{crit}$); (b) deflection softening ($\mu < \mu_{crit}$).

$$M'_{it} = 0.7425M'_{u} + 0.1739 \qquad and \quad \phi'_{it} = M'_{it} \tag{9}$$

Parameters (ϕ'_u, M'_u) represent the limit case of the moment and curvature and may be used as the ultimate values. For deflection hardening, three controlling points are needed.

$$\phi = \begin{Bmatrix} 0 \\ \phi'_{bcr} \\ \phi'_{u} \end{Bmatrix} \phi_{cr} \qquad M = \begin{Bmatrix} 0 \\ M'_{bcr} \\ M'_{u} \end{Bmatrix} M_{cr} \tag{10}$$

where normalized bilinear cracking moment curvature is equal to the intersection point, $\phi'_{bcr} = \phi'_{it}$ and $M'_{bcr} = M'_{it}$. For deflection softening, four controlling points are needed.

$$\phi = \begin{Bmatrix} 0 \\ \phi'_{bcr} \\ \phi'_{bcr} \\ \phi'_{u} \end{Bmatrix} \phi_{cr} \qquad M = \begin{Bmatrix} 0 \\ M'_{bcr} \\ M'_{cr2} \\ M'_{u} \end{Bmatrix} M_{cr} \tag{11}$$

where normalized bilinear cracking moment curvature is equal to the original normalized cracking moment curvature, $\phi'_{bcr} = \phi'_{cr} = 1$ and $M'_{bcr} = M'_{cr} = 1$. Additional normalized reduced cracking moment M'_{cr2} at normalized cracking curvature ϕ'_{cr} is obtained by linear interpolate between ϕ'_{it} and ϕ'_{u}.

$$M'_{cr2} = (1-\xi) M'_{it} + \xi M'_{u} \quad \text{where} \quad \xi = \frac{(\phi'_{cr} - \phi'_{it})}{(\phi'_{u} - \phi'_{it})} \tag{12}$$

4.2 – Specific Values when the Notched RILEM Beam is Used

If a notched RILEM TC162-TDF 3-point bending is used, the specimen can be approximated as shown in Figure 5.

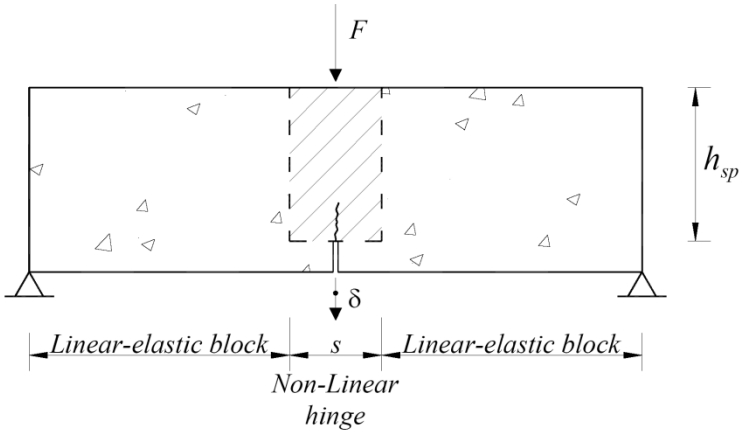

Figure 5: Specimen idealization for model use [Barros et al. 2005]. The uncracked section height, h_{unc}, equals the distance between the notch tip and the cross-section top, h_{sp}.

In this case, the following stress coefficients and strain values can be adopted [Barros et al. 2005].

$$C_1 = 0.52\,,\ C_2 = 0.36\,,\ C_2 = 0.27\,,\ \varepsilon_2 = 0.12\%\,,\ \varepsilon_3 = 10.4\%$$

4.3 – Tensile Parameters for the Un-notched Belgian Standard Beam

Contrary to the approach presented above in which case loads are recorded at deflection of 0.46 mm and 3.0 mm [Barros et al. 2005], Belgian Standard NBN B15-238 records loads at deflection of 1.5 mm and 3 mm, i.e., F_{R-15} and F_{R-30}, respectively. Corresponding residual (i.e., "equivalent") flexural strengths, f_{R-15} and f_{R-30}, are calculated as:

$$f_{R\_15} = \frac{3F_{R-15}L}{2bh_n^2}$$

$$f_{R\_30} = \frac{3F_{R-30}L}{2bh_{unc}^2}$$

In this approach it is assumed that once a beam has cracked, depth of the compressive zone equals 10% of the beam height. Hence, the equivalent flexural tensile stress in the post-cracking range can now be estimated as 37% of the corresponding linear-elastic stress. Resulting tensile stresses values σ_1, σ_2, and σ_3, as defined in Figure 1, thus equal:

$$\sigma_1 = 0.21MPa\left(\frac{f_c}{1MPa}\right)^{\frac{2}{3}}$$

$$\sigma_2 = 0.37\, f_{R\_15}$$

$$\sigma_3 = 0.37\, f_{R\_30}$$

$$\varepsilon_1 = \frac{\sigma_1}{E_c},\ \varepsilon_2 = 0.1\%\ \varepsilon_3 = 1\%$$

4.4 – Comparison with Residual Tensile Strength Results as obtained in ASTM C1399/C1399M -10 and ASTM 1609 Tests

Since the flexural design of Fiber reinforced concrete elements is generally governed by the tensile strength of the material, and assuming that the test results are interpreted correctly, the load-deformation response can be very valuable in the verification of design applications. The first objective is to make sure that the experimental results are reduced into the correct material parameters that agree with the assumptions made in model development.

ASTM C78/C78M-10 and ASTM C293/C293M -10 are based on obtaining the flexural strength results using un-notched third-point and center-point loading, respectively, as shown in Figures 6 and 7. These beam dimensions and general loading geometry have also been used to obtain the post crack tensile response using recently adopted ASTM test methods. However efforts that have attempted to correlate the uniaxial stress-strain response of FRC as described in Chapters 3 to 5, with the ASTM proposed test methods indicate that there are large differences between the test results. Currently there are no values for the stress coefficients C_1, C_2 and C_3 obtained from ASTM C1399/C1399M -10 and ASTM C1609/C1609M -10 reported in the literature. In this case the user must employ one of the standard inverse-analysis procedures described in Chapter 6 and Appendix I. For the reader's benefit, one such spreadsheet-based inverse analysis procedures is described in detail in Appendix A [Soranakom & Mobasher, 2007a,b,c], while the step-by-step process is provided in the appendix, the actual spreadsheet file can be obtained directly from the authors or the ACI 544 committee.

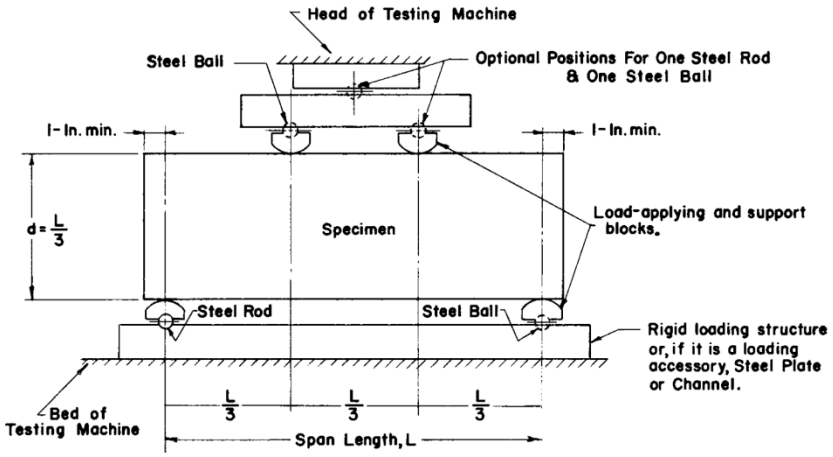

Figure 6: Third-point loading test layout used in the ASTM C78/C78M-10 method [ASTM C78/C78M-10].

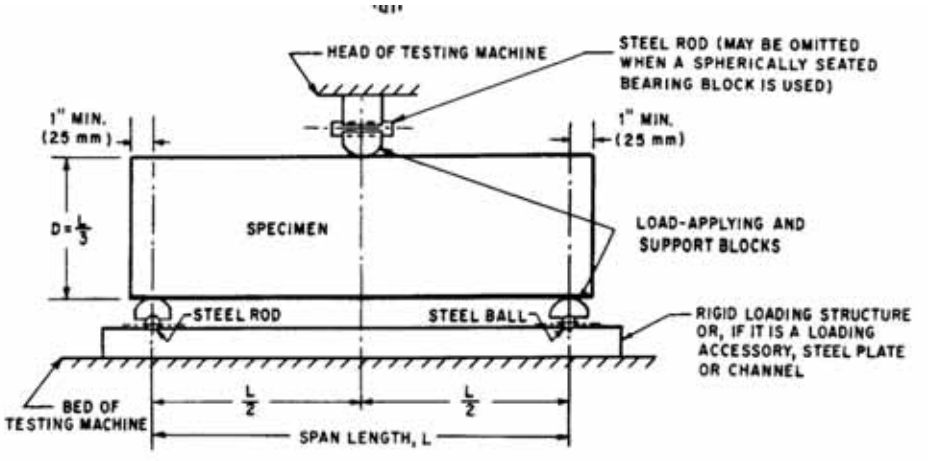

Figure 7: Center-point loading test layout used in the ASTM C293/C293M -10 method [ASTM C293/C293M -10].

The Averaged Residual Strength (ARS), proposed by Banthia and Dubey [1999, 2000] and ASTM C1399/C1399M -10 [1999], ASTM C1609/C1609M -10 [2005] is conducted by means of a load controlled test machine on a pre-cracked specimen. The post-crack strength can be obtained by a simple open loop testing machine available in many material testing laboratories. First, a steel plate is placed underneath a concrete beam and the specimen is loaded under four point bending until concrete cracks. The purpose of using steel plate in the pre-cracking process is that the load transferred onto the specimen does not diminish after cracking of the sample. The operator is expected to stop the pre-cracking loading process right after the cracking takes place. Then, the steel plate is removed and the cracked specimen is reloaded to obtain post crack flexural loads at deflection levels of 0.02, 0.03, 0.04 and 0.05 inches for specimens of 6x6x20 in (150x150x508 mm). Finally, the equivalent stress results are averaged to represent an averaged residual strength (ARS value). This parameter has been used as a method to compare different material formulations. However, many designers have been using it as a tensile strength measure. Discussions of this test method is beyond the scope of present work, however, it is noted that the ARS value is not even an equivalently elastic stress, and thus can not to be associated with the post-crack tensile strength, or tensile residual strength parameter σ_p defined in Figure 1.

ASTM C1609/C1609M -10 [1999] test is conducted on an un-notched specimen tested under deflection control. One is able to compute the post peak flexural load deflection response and utilize a method similar to ARS method proposed by ASTM C1399/C1399M -10 where load carrying capacity in the post-crack range is expressed as an equivalent stress measure. Figure 8 shows the schematics of the set-up of the two LVDTs (only one shown) used as closed loop feedback control parameters in ASTM C1609/C1609M -10.

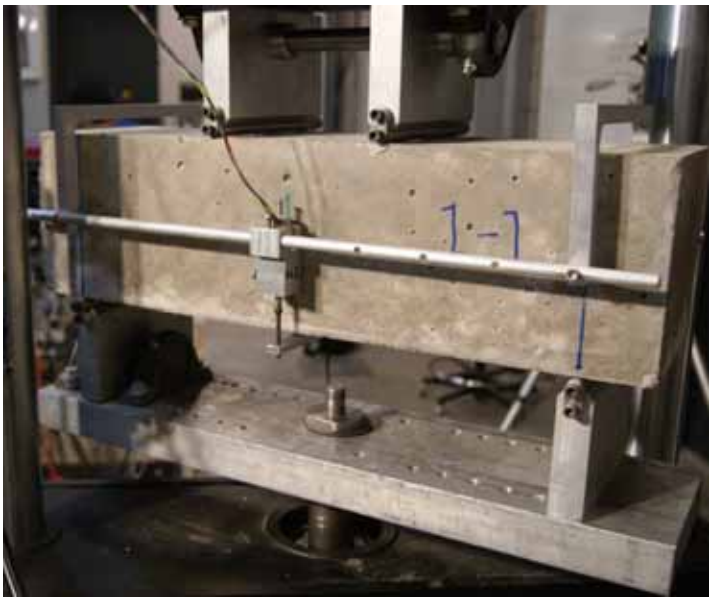

Figure 8: Crack growth in FRC samples under a three-point bending test

As the post-peak response is averaged, the residual load is used to calculate an elastically equivalent flexural stress using the section modulus of the uncracked beam. In doing so, the load is divided by the equivalent elastic section modulus. In order to show the fundamental differences with the interpretation of the test data using the two test methods, the stress distribution during the late stage of one of macro fiber sample composites is presented across the depth of the cross section in Figure 9a [Soranakom and Mobasher, 2010]. It is shown that the indirect method prediction captures the incremental movement of the neutral axis, the linear compressive stress and the residual tensile stress. According to the strain softening model, the critical post-crack tensile strength μ_{crit} = 0.35 computed from equation 6 (see Appendix A, for a value of ω=9) representing the compressive strength to tensile strength ratio) characterizes two sub classes of materials: deflection softening (μ < 0.35) and deflection hardening (μ > 0.35). The simulation of Figure 9a on Polypropylene fiber reinforced concrete reveals that the discrepancy between the present method and the Average Residual Strength Method (ARS) in accordance to the ASTM C1399/C1399M -10 or ASTM C1609/C1609M -10 is primarily due to a difference in stress distribution between the two test methods. Mobasher, B. 2011

Correlation of residual strength from ASTM C1609/C1609M -10 and the indirect methods proposed in these sections as shown in Figure 9b indicates that the ARS method overestimates the residual tensile strength by as much as three times. The inherent assumption of the ARS method is that the neutral axis is still at the centroid of the specimen and the stress distribution is linear throughout. This leads to very high nominal flexural stress levels in tension, which are far greater than the tensile strength. Extreme caution must be exercised in application of the ARS method in design and analysis of fiber reinforced concrete sections.

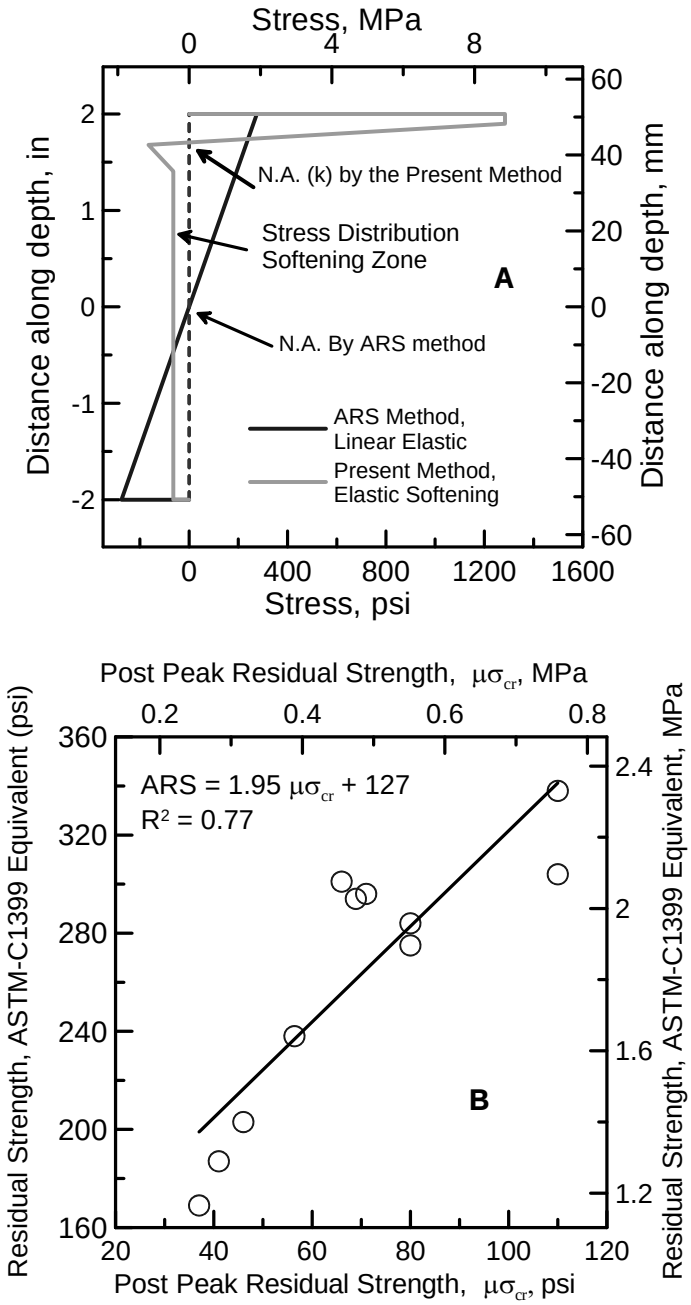

Figure 9—a) Comparison of stress distribution in the present back-calculation approach with the ARS method, b) direct correlation of residual strength from ASTM C1399/C1399M -10 and the method in Appendix A. [Soranakom and Mobasher, 2010]

CHAPTER 5 – CONCLUSIONS

This document presents existing methods for estimating uniaxial stress-strain response of strain softening FRCs using beam-test data. The methods are based on an inverse analysis of beam data. The predictive performance of the presented approaches has been experimentally validated in the cited references. The document presents both (a) a complete spreadsheet-based inverse analysis that can be used for any center-point or third-point loaded test beam, and (b) specific relationship developed by Rilem TC162-TDF committee that can be used for specific beam types presented in section 6.2. The relationship can also be used for other beam types, but the user must determine stress coefficients C_1, C_2 and C_3 using one of the described inverse analysis methods.

Finally it should be noted that the purpose of this document is to provide the reader with complete guidelines necessary for obtaining uniaxial stress-strain curves of strain softening FRCs from beam test data. To evaluate how well these methods perform as compared to experimental data, the reader is directed to the referenced publications. This document does not attempt to recommend or favour any of the presented methods. Performance and comparison of the presented methods will be discussed in future publications.

CHAPTER 6 – REFERENCES

ASTM C78/C78M-10 ASTM Committee C09 on Concrete and Concrete Aggregates, 2007, "Standard Test Method for Flexural Strength of Concrete (Using Simple Beam with Third-Point Loading)," *ASTM International*.

ASTM C293/C293M-10 ASTM Committee C09 on Concrete and Concrete Aggregates, 2007 "Standard Test Method for Flexural Strength of Concrete (Using Simple Beam with Center-Point Loading)*," ASTM International*.

ASTM C1399/C1399M-10 ASTM Committee C09 on Concrete and Concrete Aggregates, 2007, "Standard Test Method for Obtaining Average Residual-Strength of Fiber-Reinforced Concrete*," ASTM International*.

ASTM C1609/C1609M-10 ASTM Committee C09 on Concrete and Concrete Aggregates, 2007, "Standard Test Method for Flexural Performance of Fiber-Reinforced Concrete," *ASTM International*.

Banthia 1995 a Banthia, N. and Trottier, J.F., 1995, "Test Methods for Flexural Toughness Characterization of Fiber Reinforced Concrete: Some Concerns and a Proposition,". *ACI Materials Journal*, Vol. 92, No. 1, pp. 48-57.

Banthia 1995 b Banthia, N. and Trottier, J.F., 1995, "Concrete reinforced with deformed steel fibres, Part II: Toughness characterization," *ACI Materials Journal*, Vol. 92, No. 2, pp. 146-154.

Banthia 1999 Banthia, N., and Dubey, A., 1999, "Measurement of Flexural Toughness of Fiber-Reinforced Concrete Using a Novel Technique - Part 1: Assessment and Calibration," *ACI Materials Journal*, Vol. 96, No. 6, pp. 651-656.

Banthia 2000 Banthia, N., and Dubey, A., 2000, "Measurement of Flexural Toughness of Fiber-Reinforced Concrete Using a Novel Technique - Part 2: Performance of various composites," *ACI Materials Journal*, Vol. 97, No. 1, January/February, pp. 3-11.

Barragán 2002 Barragán, B.E., 2002. *Failure and toughness of steel fiber reinforced concrete under tension and shear*, PhD Thesis, UPC, Barcelona.

Barros 2004 Barros, J.A.O., Pereira, E.B., Ribeiro, A.F., and Antunes J.A.B., 2004, "Self-compacting steel fibre reinforced concrete for precasted sandwich panels – experimental and numerical research", *Workshop of 6th International RILEM Symposium on fibre reinforced concrete - BEFIB 2004*, 24-25 September 2004.

Barros 2005 Barros, J. A. O., Cunha, V. M. C. F., Ribeiro, A. F., and Antunes, J. A. B., 2005, "Post-cracking Behaviour of Steel Fibre Reinforced Concrete," *Materials and Structures*, Vol. 38, 47-56.

ENV 1992 ENV 1992-1-1, 1992, *Eurocode 2: Design of concrete structures - Part 1: General rules and rules for buildings*. Technical report, European pre-standard.

Gopalaratnam 1991 Gopalaratnam, V.S. *et al.*, 1991, Fracture Toughness of Fiber Reinforced Concrete," *ACI Materials Journal*, Vol. 88, No. 4, pp. 339-353.

Hillerborg 1908 Hillerborg, A., 1980, "Analysis of Fracture by Means of the Fictitious Crack Model, Particularly for Fibre Reinforced Concrete", *The International Journal of Cement Composites*, Vol. 2, No. 4, pp. 177-184.

JSCE 1984 Japan Society of Civil Engineers, 1984, "Method of Test for Flexural Strength and Flexural Toughness of Fiber Reinforced Concrete," *Standard SF-4*: 58-66.

Taheri et al. 2011 Taheri, M.; Barros, J.A.O.; Salehian, H.R., 2011, "A Design Model for Strain-Softening and Strain-Hardening Fiber Reinforced Elements Reinforced Longitudinally with Steel and FRP Bars", *Composites - part B Journal*, Vol. 42, pp. 1630-1640.

Mobasher, B. 2011 Mobasher B., 2011, *Mechanics of fiber and textile reinforced cement composites*, pp. 450, CRC Press, Boca Raton, FL.

Naaman et al 2005 Naaman, A.E., and Reinhardt, H. W., 2005, "Proposed Classification of HPFRC composites Based on Their Tensile Response," *Construction Materials*, Proceedings of the *3rd International Conference on Construction Materials: Performance, Innovations and Structural Implications - ConMat '05 and Mindess Symposium*, The University of British Columbia, pp. 458.

Noghabai 1998 Noghabai, K., 1998, *Effect of Tension Softening on the Performance of Concrete Computational Studies*, PhD Thesis, Dept. of Civil and Mining Eng., Division of Structural Eng., Lülea University of Technology, Sweden.

Nemegeer 1998 Nemegeer-Harelbeke, D., 1998, *Design Guidelines for Dramix Steel Fibre Reinforced Concrete*, Bekaert.

Schellekens 1990 Schellekens, J., 1990, "Interface elements in finite element analysis", *TU-Delft Report 25.2-90-5-17/TNO-IBBC,* Report BI-90-165.

Soranakom 2007 a Soranakom, C., and Mobasher, B., 2007, "Closed-Form Moment-Curvature Expressions For Homogenized Fiber Reinforced Concrete," *ACI Materials Journal*, Vol. 104, No. 4, July-August.

Soranakom 2007 b Soranakom, C., and Mobasher, B., 2007, "Closed Form Solutions for Flexural Response of Fiber Reinforced Concrete Beams," *ASCE Journal of Engineering Mechanics*, Volume 133, Issue 8, August.

Soranakom 2007 c Soranakom, C. and Mobasher, B. 2007, "Flexural Modeling of Strain Softening and Strain Hardening Fiber Reinforced Concrete," H.W. Reinhardt and A.E. Naaman, Co-Editors, *High Performance Fiber Reinforced Cement Composites - HPFRCC 5,* RILEM Proceedings, Pro. 53, S.A.R.L., Cachan, France, pp. 155-164.

Soranakom 2008 a Soranakom, C., and Mobasher, B., 2008, "Moment-Curvature Response of Strain Softening and Strain Hardening Cement Based Composites," *Cement and Concrete Composites,* Vol. 30, Issue 6, pp. 465-477, July.

Soranakom 2008 b Soranakom, C., Yekani-Fard, M., and Mobasher, B., 2008, "Development of Design Guidelines For Strain Softening Fiber Reinforced Concrete," *7th International Symposium of Fiber Reinforced Concrete: Design and Applications BEFIB 2008*, Editor: R. Gettu, September, pp 513-523.

Soranakom 2009 a Soronakom, C., and Mobasher B., 2009, "Design Flexural Analysis and Design of Textile Reinforced Concrete," *Textile Reinforced Structures: Proceedings of the 4nd Colloquium on Textile Reinforced Structures (CTRS4) und zur 1.*

Anwendertagung, SFB 528, Technische Universität Dresden, Eigenverlag, ISBN 978-3-86780-122-5, pp. 273-288.

Soranakom 2009 b — Soranakom, C., and Mobasher, B., 2009, "Flexural Design of Fiber Reinforced Concrete," *ACI Materials Journal*, September-October, pp. 461-469

Soranakom 2010 — Soronakom, C., and Mobasher B., 2010, "Flexural Analysis and Design of Strain Softening Fiber Reinforced Concrete," ACI-SP-272, Editors, G.J. Para-Montesinos, P. Balaguru, pp. 173-187.

Vandewalle 2000 a — Vandewalle, L. et al., 2000, "Test and Design Methods for Steel Fiber Reinforced Concrete – Recommendations for Bending Tests," *Materials and Structures*, Vol. 33, No. 225, January-February, pp. 3-5.

Vandewalle 2000 b — Vandewalle, L. *et al.* 2000, "Test and Design Methods for Steel Fiber Reinforced Concrete - Recommendations for σ-ε Design Method," *Materials and Structures*, Vol. 33, No. 226, pp. 75-81.

Vandewalle 2002 a — Vanderwalle, L. et al., 2002, "Design of Steel Fibre Reinforced Concrete Using σ-w Method: Principles and Applications," *Materials and Structures Journal*, Vol. 35, pp. 262-278, June.

Vandewalle 2002 b — Vandewalle, L. et al., 2002, "Test and Design Methods for Steel Fiber Reinforced Concrete – Final Recommendation," *Materials and Structures*, Vol. 35, No. 253, November, pp. 579 - 582.

Vandewalle 2003 — Vandewalle, L. et al., 2003, "Test and Design Methods for Steel Fiber Reinforced Concrete – s-e Design Method – Final Recommendation," *Materials and Structures*, Vol. 36, No. 262, October, pp. 560 – 567.

APPENDIX A: SPREADSHEET-BASED INVERSE ANALYSIS PROCEDURE

A.1 – Derivation of the Moment-Curvature Diagram

Moment curvature diagram is derived by first drawing stress strain diagram according to the applied normalized compressive strain at the top fiber λ in 3 stages: (0<λ≤1), (1<λ≤ω) and (ω<λ≤λ_{cu}). The neutral axis depth ratio *k* is then found by solving equilibrium of forces. Finally the moment capacity is calculated by taking tension and compression forces around the neutral axis and the corresponding curvature is obtained by dividing the top compressive strain with the neutral axis depth. Moment *M* and curvature ϕ are then normalized with their cracking moment M_{cr} and cracking curvature ϕ_{cr} to obtained a normalized moment *M'* and curvature ϕ', respectively. Note that, from now on, the primed terms (*M' or* ϕ') refer to the normalized quantities with respect to cracking moment M_{cr} or cracking curvature ϕ_{cr}. For example $M'_{cr} = M_{cr}/M_{cr} = 1$ and $\phi'_{cr} = \phi_{cr}/\phi_{cr} = 1$. The expressions for calculating moment curvature and neutral axis for three stages of applied top compressive strain λ are given in Eq. (1) - (5).

$$M(\lambda,k,\omega,\mu) = M_{cr}\, M'(\lambda,k,\omega,\mu) \qquad M_{cr} = \frac{1}{6} bd^2 E\varepsilon_{cr} \tag{1}$$

$$\phi(\lambda,k,\omega,\mu) = \phi_{cr}\, \phi'(\lambda,k,\omega,\mu) \qquad \phi_{cr} = \frac{2\varepsilon_{cr}}{d} \tag{2}$$

$$M'(\lambda,k,\omega,\mu) = \begin{cases} \dfrac{\lambda}{2k} & \text{for} \quad 0 \le \lambda \le 1 \\ \dfrac{(2\lambda^3 + 3\mu\lambda^2 - 3\mu + 2)k^2}{\lambda^2} - 3\mu(2k-1) & \text{for} \quad 1 < \lambda \le \omega \\ \dfrac{(3\mu\lambda^2 + 3\omega\lambda^2 - 3\mu - \omega^3 + 2)k^2}{\lambda^2} - 3\mu(2k-1) & \text{for} \quad \omega < \lambda \le \lambda_{cu} \end{cases} \tag{3}$$

$$\phi'(\lambda,k,\omega,\mu) = \frac{\lambda}{2k} \qquad \text{for} \quad 0 < \lambda \le \lambda_{cu} \tag{4}$$

$$k = \begin{cases} \dfrac{1}{2} & \text{for} \quad 0 \le \lambda \le 1 \\ \dfrac{2\mu\lambda}{\lambda^2 + 2\mu(\lambda+1) - 1} & \text{for} \quad 1 < \lambda \le \omega \\ \dfrac{2\mu\lambda}{-\omega^2 + 2\lambda(\omega+\mu) + 2\mu - 1} & \text{for} \quad \omega < \lambda \le \lambda_{cu} \end{cases} \tag{5}$$

For a given set of material parameters and dimension of the beam section, the moment curvature diagram can be generated by substituting an incremental normalized top compressive strain λ from zero up to failure in Eq. (1) - (5). Two possible moment curvature responses, deflection hardening ($\mu > \mu_{crit}$) and deflection softening ($\mu < \mu_{crit}$), are shown by solid curves in Figure 6. The critical value for normalized post peak tensile strength is given in Eq. (6).

$$\mu_{crit} = \frac{\omega}{3\omega - 1} \tag{6}$$

In calculation of moment curvature diagram, the ultimate normalized top compressive strain λ_u needs to be identified by comparing the normalized top compressive strain at compressive failure λ_{cu} and the normalized top compressive strain at tensile failure λ_{tu}. The smaller of these two limits the flexural capacity.

$$\lambda_u = \min\left(\lambda_{cu}, \lambda_{tu}\right) \tag{7}$$

where

$$\lambda_{tu} = \begin{cases} \sqrt{2\mu\beta_{tu} - 2\mu + 1} & \text{stage 2, } 1 < \lambda \le \omega, \quad \text{when } \beta_{tu} \le \dfrac{\left(\omega^2 + 2\mu - 1\right)}{2\mu} \\ \dfrac{2\mu\beta_{tu} - 2\mu + \omega^2 + 1}{2\omega} & \text{stage 3,} \quad \lambda > \omega, \quad \text{when } \beta_{tu} > \dfrac{\left(\omega^2 + 2\mu - 1\right)}{2\mu} \end{cases} \tag{8}$$

The normalized ultimate moment M'_u is then be found by using Eq (3), (5), (7) and (8). Table A1 presents a summary of the neutral axis depth, the normalized moment, and the curvature for general loading condition as a function of various tensile post peak strength levels, μ.

A.1.1 – Simplified Moment Curvature Diagram

Figure 6 shows the simplification of normalized moment curvature diagrams to normalized bilinear moment curvature diagrams for deflection hardening and deflection softening. In the simplified models, the intersection points (ϕ'_{it}, M'_{it}) of the linear elastic response and the linear post crack response is found by using a regression equation (9). Note that the regression equation is dimensionless, independent of the unit used.

$$M'_{it} = 0.7425M'_{u} + 0.1739 \qquad and \qquad \phi'_{it} = M'_{it} \tag{9}$$

For deflection hardening, three controlling points are needed.

$$\phi = \begin{Bmatrix} 0 \\ \phi'_{bcr} \\ \phi'_{u} \end{Bmatrix} \phi_{cr} \qquad M = \begin{Bmatrix} 0 \\ M'_{bcr} \\ M'_{u} \end{Bmatrix} M_{cr} \tag{10}$$

where normalized bilinear cracking moment curvature is equal to the intersection point, $\phi'_{bcr} = \phi'_{it}$ and $M'_{bcr} = M'_{it}$. For deflection softening, four controlling points are needed.

$$\phi = \begin{Bmatrix} 0 \\ \phi'_{bcr} \\ \phi'_{bcr} \\ \phi'_{u} \end{Bmatrix} \phi_{cr} \qquad M = \begin{Bmatrix} 0 \\ M'_{bcr} \\ M'_{cr2} \\ M'_{u} \end{Bmatrix} M_{cr} \tag{11}$$

where normalized bilinear cracking moment curvature is equal to the original normalized cracking moment curvature, $\phi'_{bcr} = \phi'_{cr} = 1$ and $M'_{bcr} = M'_{cr} = 1$. The additional normalized reduced cracking moment M'_{cr2} at normalized cracking curvature ϕ'_{cr} is obtained by linear interpolate between ϕ'_{it} and ϕ'_{u}.

$$M'_{cr2} = (1-\xi) M'_{it} + \xi M'_{u} \qquad \text{where} \qquad \xi = \frac{(\phi'_{cr} - \phi'_{it})}{(\phi'_{u} - \phi'_{it})} \qquad (12)$$

A.1.2 – Load – Deflection Response

Figure A1 shows the set up for three and four point bending tests. Figures A1(b) and (c) show their moment distributions at cracking and ultimate levels. With the area moment method, the corresponding curvature diagrams shown in Figures A1 (c) - (e) are divided into several areas and taken around the left support to obtain the mid-span deflection δ. A set of equations for calculating mid span deflection of three point bending at first bilinear cracking, at ultimate when material has $\mu > \mu_{crit}$, and at ultimate when material has $\mu < \mu_{crit}$ are presented in Eqs. 12(a) – 12(c).

Table A1 - Representations for the depth of Neutral axis, Moment and curvature as a function of applies strain beyond the first cracking point ($\lambda = \varepsilon / \varepsilon_{cr}$) bilinear compression, bilinear tension

		ω	μ=1	μ=0.75	μ=0.5	μ=0.25	μ=0.1
κ	$\frac{-2\mu\lambda}{\omega^2-2\omega\lambda-2\mu\lambda-2\mu+1}$	1	$\frac{1}{2}$	$\frac{1.5\lambda}{3.5\lambda-0.5}$	$\frac{\lambda}{3\lambda-1}$	$\frac{\lambda}{5\lambda-3}$	$\frac{0.2\lambda}{2.2\lambda-1.8}$
		5	$\frac{\lambda}{6\lambda-12}$	$\frac{1.5\lambda}{11.5\lambda-24.5}$	$\frac{\lambda}{11\lambda-25}$	$\frac{\lambda}{21\lambda-51}$	$\frac{0.2\lambda}{10.2\lambda-25.8}$
M	$\frac{\left(3(\omega+\mu)\lambda^2-\omega^3-3\mu+2\right)\kappa^2}{\lambda^2}-6\mu\kappa+3\mu$	1	$\frac{3\lambda^2-1}{2\lambda^2}$	$\frac{3(17\lambda^2-4\lambda-1)}{(7\lambda-1)^2}$	1.	$\frac{15\lambda^2-18\lambda+7}{(5\lambda-3)^2}$	$\frac{33\lambda^2-54\lambda+25}{(11\lambda-9)^2}$
		5	$\frac{(0.5\lambda^2-20\lambda+17)}{2(\lambda-2)^2}$	$\frac{3(245\lambda^2-980\lambda+827)}{(23\lambda-49)^2}$	$\frac{3(55\lambda^2-250\lambda+271)}{(11\lambda-25)^2}$	$\frac{35\lambda^2-170\lambda+203}{(7\lambda-17)^2}$	$\frac{85\lambda^2-430\lambda+541}{(17\lambda-43)^2}$
φ	$\frac{\lambda}{2\kappa}$	1	1	$\frac{3.5\lambda-0.5}{3}$	$\frac{3\lambda-1}{2}$	$\frac{5\lambda-3}{2}$	$\frac{22\lambda-18}{4}$
		5	$3\lambda-6$	$\frac{11.5\lambda-24.5}{3}$	$\frac{11\lambda-25}{2}$	$\frac{21\lambda-51}{2}$	$\frac{10.2\lambda-25.8}{0.4}$

$$\delta_{bcr} = \frac{1}{12} L^2 \phi_{bcr} \tag{13.a}$$

$$\delta_u = \frac{L^2}{24 M_u^2}\left[\left(2M_u^2 - M_u M_{bcr} - M_{bcr}^2\right)\phi_u + \left(M_u^2 + M_u M_{bcr}\right)\phi_{bcr}\right] \qquad \mu > \mu_{crit} \tag{13.b}$$

$$\delta_u = \frac{\phi_u L_p}{8}\left(2L - L_p\right) + \frac{M_u \phi_{bcr} L}{12 M_{bcr}}\left(L - 2L_p\right) \qquad \mu < \mu_{crit} \tag{13.c}$$

Similarly, a set of equations for four point bending can be written as:

$$\delta_{bcr} = \frac{23}{216} L^2 \phi_{bcr} \tag{14.a}$$

$$\delta_u = \frac{L^2}{216 M_u^2}\left[\left(23M_u^2 - 4M_u M_{bcr} - 4M_{bcr}^2\right)\phi_u + \left(4M_u^2 + 4M_u M_{bcr}\right)\phi_{bcr}\right] \qquad \mu > \mu_{crit} \tag{1.b}$$

$$\delta_u = \frac{5L^2 \phi_u}{72} + \frac{M_u L^2 \phi_{bcr}}{27 M_{bcr}} \qquad \mu < \mu_{crit} \tag{2.c}$$

Load step P_i can be back calculated from a discrete point i along the moment curvature diagram as follows.

$$P_i = \frac{2M_i}{S} \qquad \text{for } \phi_i = 0 \ldots \phi_u \tag{20}$$

where S is a spacing between the support and loading point, $S=L/2$ for three point bending and $S=L/3$ for four point bending.

A.1.3 – Example: Three Point Bending Test

Determine the moment curvature diagram and load deflection response of a beam size 100x100 mm tested under three point bending at clear span L = 300 mm. Assume that the plastic length for crack localized zone under the point load L_p=100 mm. The ultimate uniaxial compressive strength f'_c= 30 MPa,

uniaxial tensile strength σ_{cr} = 2.50 MPa and post peak tensile strength σ_p = 0.75 MPa. The ultimate compressive strain ε_{cu} = 0.003 and the ultimate tensile strain ε_{tu} = 0.02. The Young modulus E = 25,000 MPa.

Step one- Using the specified material properties determine the normalized material parameters. These parameters can be calculated as follows.

Cracking strain $\varepsilon_{cr} = \sigma_{cr}/E$ = 2.5/25000 = 0.0001

Normalized post peak tensile strength, $\mu = \sigma_p/\sigma_{cr}$ = 0.75/2.5 = 0.30

Normalized ultimate tensile strain, $\beta_{tu} = \varepsilon_{tu}/\varepsilon_{cr}$ = 0.02/0.0001 = 200

Normalized ultimate compressive strain, $\lambda_{cu} = \varepsilon_{cu}/\varepsilon_{cr}$ = 0.003/0.0001 = 30

Assumed compressive yield stress $\sigma_{cy} = 0.8*fc' =$ 0.8*30 = 24 MPa

Compressive to tensile strain ratio, $\omega = \sigma_{cy}/(E\varepsilon_{cr})$ = 24/2.5 = 9.6

In the Excel worksheet, users can enter these input parameters in the green highlighted cells. Other cells will automatically calculate according to the user input. The unit used is a consistent unit, hence it does not matter if English system or SI system is used, however consistency must be maintained.

From the information given above, use the following additional information in the excel spreadsheet: *test method* = 3, b = 100 mm, d = 100 mm, L = 300 mm, L_p=100 mm, E = 25000 MPa.

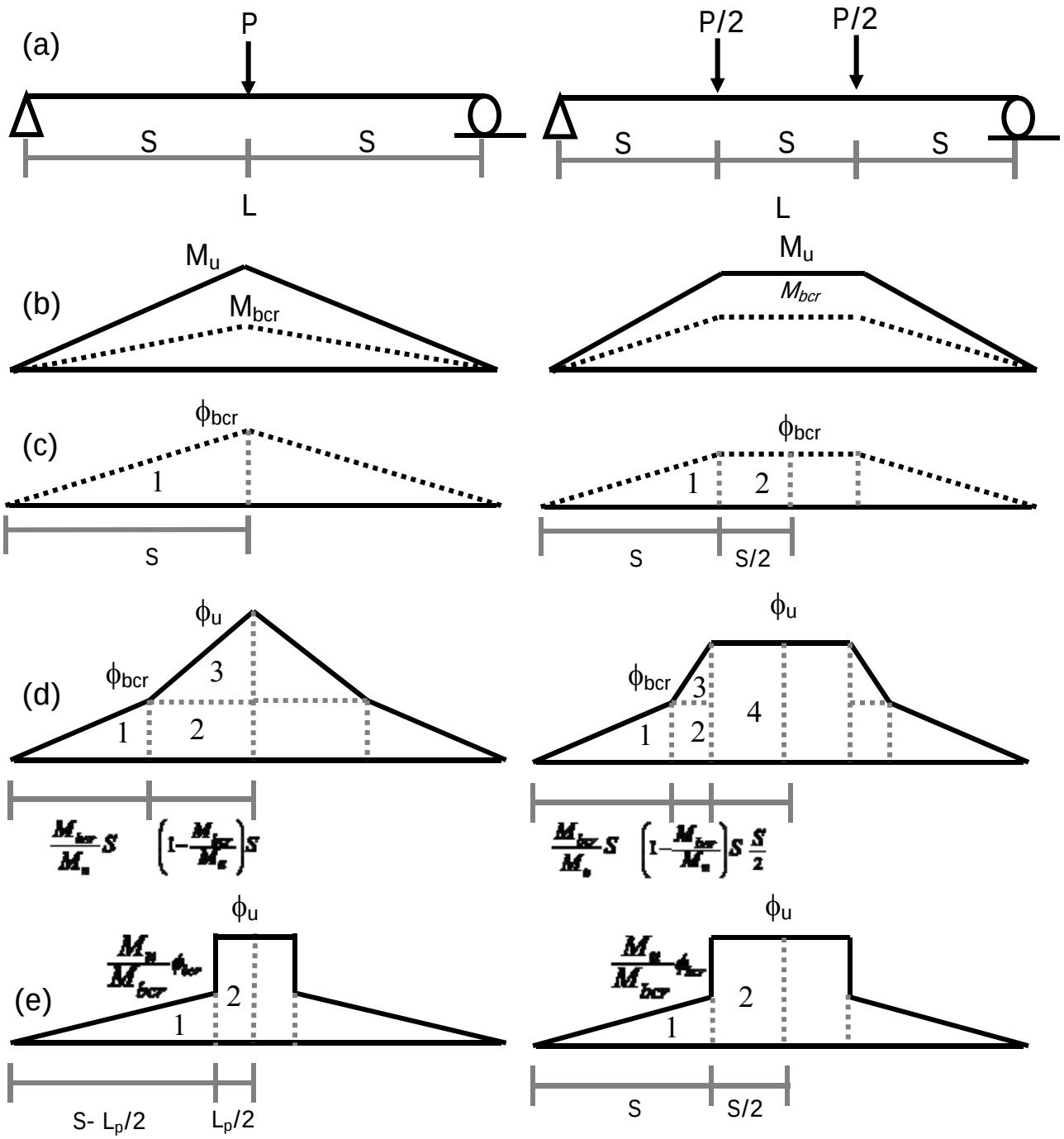

Figure A1: Three and four point bending test: (a) Experimental setup; (b) Moment distribution; (c) Curvature distribution at first bilinear cracking; (d) Curvature distribution at ultimate moment for high normalized post peak tensile strength ($\mu > \mu_{crit}$); (e) Curvature distribution at ultimate moment for low normalized post peak tensile strength ($\mu < \mu_{crit}$).

According to the material parameters input, the tensile and compressive stress strain responses are calculated and plotted in Figure A2. The critical normalized post peak tensile strength μ_{crit}=0.345 is calculated by Eq. (6).

$$\mu_{crit} = \frac{\omega}{3\omega - 1} = \frac{9.6}{3(9.6) - 1} = 0.345$$

Since μ = 0.30 ' < μ_{crit} , the worksheet shows type 2 (deflection softening). According to the normalized ultimate tensile failure β_{tu}, the corresponding normalized top compressive strain λ_{tu} is checked by Eq. (8), which shows that the compressive strain fails at stage 3 ($\omega < \lambda$).

$$\beta_{\mathrm{tu}} = 200 > \frac{\left(\omega^2 + 2\mu - 1\right)}{2\mu} = \frac{\left(9.6^2 + 2*0.3 - 1\right)}{2*.6} = 159$$

$\lambda_{tu} < \lambda_{cu}$ means that the ultimate tensile strain will reach the failure before the compressive strain crushing. The smaller of λ_{tu} (=11.03) and λ_{cu} *(=30)* is used as a normalized ultimate compressive strain λ_u in the calculation of neutral axis depth ratio k_u by Eq. (5).

$$k_u = \frac{2\mu\lambda}{-\omega^2 + 2\lambda(\omega + \mu) + 2\mu - 1} = 0.052$$

$$M'(\lambda, k, \omega, \mu) = \frac{(3\mu\lambda^2 + 3\omega\lambda^2 - 3\mu - \omega^3 + 2)k^2}{\lambda^2} - 3\mu(2k - 1) = 0.868 \quad (3)$$

$$\phi'(\lambda, k, \omega, \mu) = \frac{\lambda}{2k} = \frac{11.03}{2(0.052)} = 105.52$$

The normalized ultimate moment M'_u and curvature ϕ'_u are calculated by Eqs. (3) and (4), respectively as 0.868, and 105.52. The intersection points (ϕ'_{it}, M'_{it}) of the linear elastic and the linear post crack response for bilinear moment curvature diagram is found by regression Eq. (9). The normalized cracking moment curvature always equal to one, ($\phi'_{cr} = M'_{cr} = 1$). Because the material is deflection softening, the normalized reduced cracking moment M'_{cr2} is needed and calculated by Eq. (12) as 0.818. The four controlling points for deflection softening moment curvature diagram for Eq. (11) are completed.

$$\phi'_{it} = M'_{it} = 0.7425M'_{u} + 0.1739 \quad = 0.7425(0.868) + 0.1739 = 0.818$$

The four controlling points for normalized moment and curvature, and dimensionalized moment and curvature in addition to the computed load and deflection values for these control points are obtained as:

Table 2 - Normalized moment and curvature, and dimensionalized moment and curvature in addition to the computed load and deflection values for the example case of A1

ϕ'	M'	ϕ, 1/mm	M, Nmm	δ, mm	P, N
0.000	0.000	0.000E+00	0	0.0000	0
1.000	1.000	2.000E-06	416,667	0.0150	5,556
1.000	0.818	2.000E-06	340,929	0.0150	4,546
105.521	0.868	2.110E-04	361,528	1.3234	4,820

The moment curvature response is recovered by multiplying the cracking moment curvature to their normalized moment curvature using Eqs. (1), (2) and (11). The deflections of three point bending for the deflection softening $\mu<\mu_{crit}$ are calculated by Eqs. 13(a), 13(c) and the load is calculated by Eq. (20). Note that the deflections at the cracking are the same but the load step due to M_{bcr} and M_{cr2} are different.

Alternatively, the accurate moment curvature diagram can be done directly by using Eqs. (1) - (8). Figure A3 compares the accurate moment curvature diagram and their approximate bilinear models. The load deflection response according to bilinear models is shown in Figure A4.

For four point bending test, the procedure is almost the same except that L_p is not needed, users can enter any value or simply zero.

An accurate expression for moment curvature can be developed using the closed form equations identifying each one of the three zones of response. The computed data presented in tabular form is presented in Table 3.

Accurate Moment Curvature Diagram						
stage	λ	k	ϕ'	M'	ϕ	M
1	0.00	0.500	0.000	0.000	0.00E+00	0
1	1.00	0.500	1.000	1.000	2.00E-06	416,667
2	1.86	0.267	3.480	0.772	6.96E-06	321,519
2	3.15	0.166	9.510	0.802	1.90E-05	334,339
2	5.30	0.103	25.725	0.837	5.15E-05	348,761
2	7.45	0.075	49.644	0.854	9.93E-05	355,836
2	9.60	0.059	81.267	0.864	1.63E-04	359,936
3	9.97	0.057	87.334	0.865	1.75E-04	360,432
3	10.34	0.055	93.401	0.866	1.87E-04	360,835
3	10.70	0.054	99.468	0.867	1.99E-04	361,166
3	11.07	0.052	105.535	0.867	2.11E-04	361,442

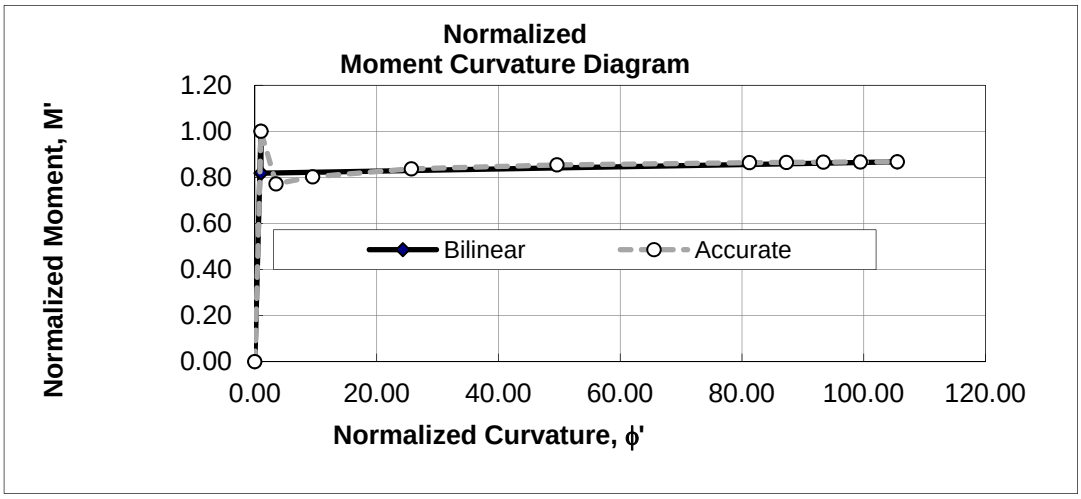

5

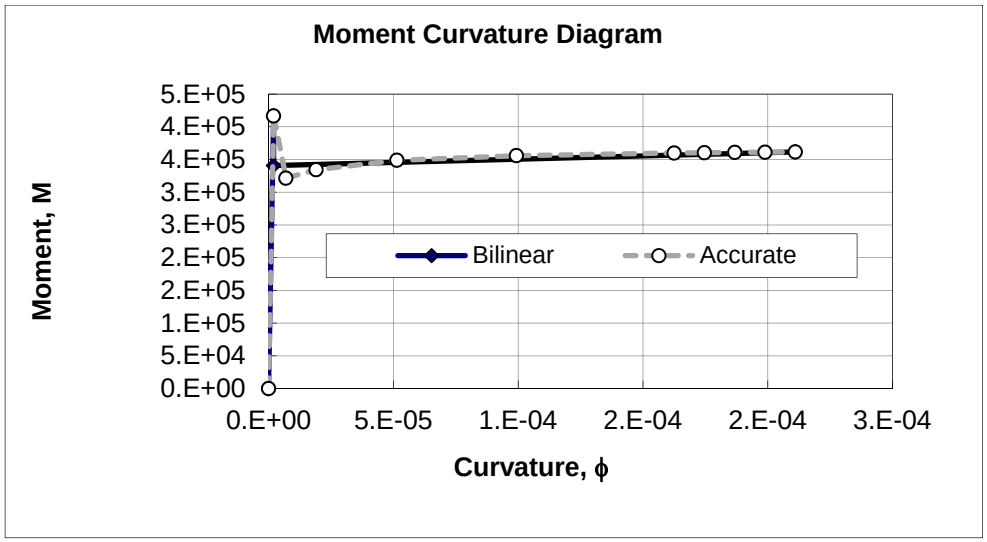
Moment Curvature Diagram
Moment, M
5.E+05
4.E+05
4.E+05
3.E+05
3.E+05
2.E+05
2.E+05
1.E+05
5.E+04
0.E+00
Bilinear
Accurate
0.E+00
5.E-05
1.E-04
2.E-04
2.E-04
3.E-04
Curvature, ϕ

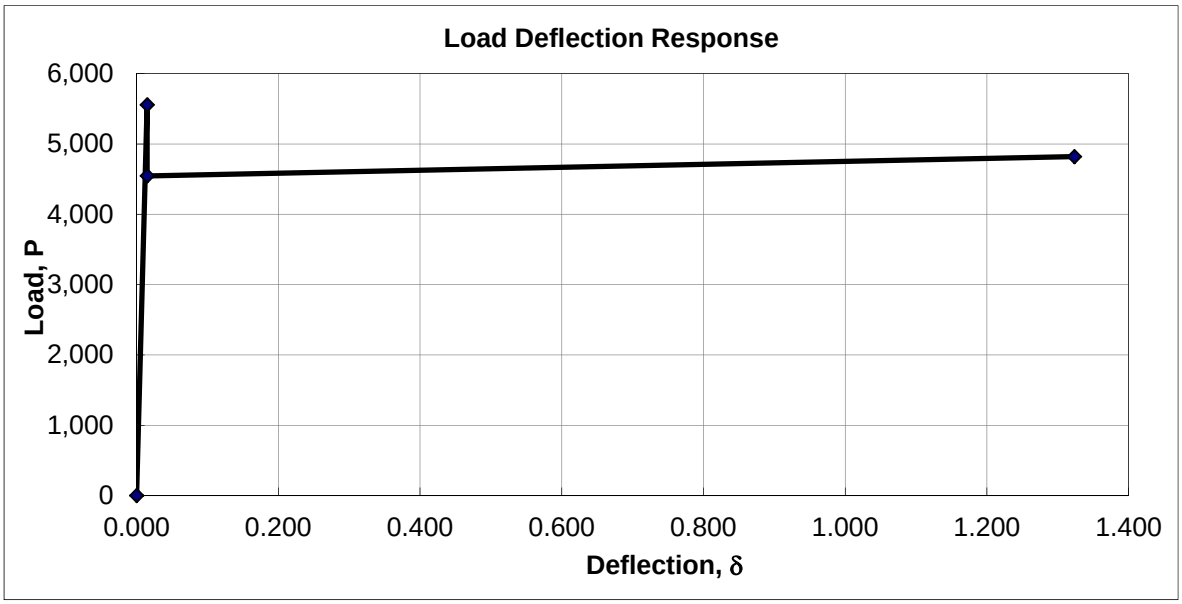
Load Deflection Response
Load, P
6,000
5,000
4,000
3,000
2,000
1,000
0
0.000
0.200
0.400
0.600
0.800
1.000
1.200
1.400
Deflection, δ

Figure A2